# Many-Body Theory of the Magnetic Hyperfine Interaction in the Excited State ($1s\,^2 2s\,2p\,^3P$) of the Beryllium Atom*

S. N. Ray, Taesul Lee, and T. P. Das
*Department of Physics, State University of New York at Albany, Albany, New York 12222*
(Received 22 August 1972)

The hyperfine interaction in the ($1s\,^2 2s 2s\,^3P_2$) excited state of the beryllium atom is of interest since it is the lowest excited state in which hyperfine effects can occur, the ground state being a singlet. In the present work the magnetic hyperfine interaction for $Be^9$ is studied theoretically using the linked cluster many-body perturbation theory including up to second order in the electron-electron interaction, certain classes of ladder diagrams, and selected third-order diagrams. Our theoretical value of $A$ in $A\vec{I}\cdot\vec{J}$ is composed of $-107.41$ MHz from the zero-order valence $2s$ and $2p$ electrons and $-16.80$ MHz from higher-order diagrams the total value $-124.21$ MHz being in good agreement with the experimental result of $-124.5368 \pm 0.0017$ MHz. The contributions from various diagrams are interpreted in terms of physical effects such as exchange core-polarization and correlation effects, the influence of $2s2p$ interactions being significant in influencing the hyperfine constant.

## I. INTRODUCTION

The linked-cluster many-body perturbation theory (LCMBPT) developed by Brueckner and Goldstone (BG)[1] has been applied successfully to the study of hyperfine properties of a number of atomic systems.[2-7] The LCMBPT procedure seems especially suitable to the hyperfine structure (hfs) problem both because the wave function is an eigenfunction of $\vec{S}^2$ to all orders and also because it enables a convenient separation of physical effects, such as core polarization and various types of correlation.

The study of hyperfine interactions in excited states of group-II (alkaline earth) atoms is of interest since the ground state is a singlet and hence, there is no hyperfine effect, and one has to go to the excited state to observe the latter. The group-II elements fall into this category, and we have started a program for study of their hyperfine interactions in $^3P$ states. In the present paper, we would like to report on our LCMBPT investigations of the magnetic hyperfine interaction for the excited ($1s^2 2s2p$) state of beryllium atom.

From a many-body point of view, the excited state of beryllium has some unique features. The unpaired $2s$ and $2p$ states are expected to correlate strongly, and it is interesting to investigate the effect of this correlation on their contributions to the hfs. This situation is different from boron and nitrogen which also have $2s$ electrons but in paired states, leading to a near cancellation between $1s$ and $2s$ core-polarization effects. The beryllium system also has some similarities with the lithium atom ground and excited states in having only one paired core state ($1s$), whereas, the latter systems have either a $2s$ electron or a $2p$ alone, both are simultaneously present in beryllium.

The magnetic dipole hyperfine constants in this system are available from recent atomic-beam measurements,[8] and will be compared with our theoretical results. In a subsequent investigation, we will utilize the same basis set and some of the matrix elements utilized here to derive the nuclear quadrupole moment of $Be^9$ from atomic-beam nuclear-quadrupole-coupling data, a quantity of great current interest for interpretation of solid-state nuclear-quadrupole data.

In Sec. II, we present a brief description of the procedure we have used. Section III presents the contributions from different hyperfine diagrams. Finally, Sec. IV presents a discussion and comparison of our results with experiment and earlier theoretical calculations, mainly one electron in nature.

## II. DESCRIPTION OF PROCEDURE

Since these have been discussed in detail in the literature,[4,6] we shall present only a brief résumé of the LCMBPT theory at the beginning of this section. This is followed by a discussion of the $V^{N-1}$ potential and basis sets that we have used. Section IID deals with the description of the pertinent diagrams for contact, dipolar, and orbital hyperfine operators. Numerical details and results are presented in Sec. III.

### A. Resumé of BG Theory

The nonrelativistic exact Hamiltonian for an atomic system of $N$ electrons can be written

$$\mathcal{H} = \sum_{i=1}^{N} T_i + \sum_{i<j} V_{ij}\,, \tag{1}$$

where $T_i$ stands for the sum of the kinetic energy and nuclear Coulomb potential of the $i$th electron, and $V_{ij}$ is the electrostatic interaction potential between electrons $i$ and $j$. For studying the atomic properties, one is interested in the exact solution

of the Schrödinger equation

$$\mathcal{H}\Psi_0 = E\Psi_0 \ . \tag{2}$$

In the perturbation procedure used here, $\mathcal{H}$ is replaced by a central-field-approximation Hamiltonian

$$\mathcal{H}_0 = \sum_{i=1}^{N} (T_i + V_i) \ , \tag{3}$$

and $\mathcal{H}' = \mathcal{H} - \mathcal{H}_0$ is treated as a small perturbation. The single-particle potential $V_i$ is selected in such a way that the one-electron equation

$$(T + V)\varphi_i = \epsilon_i \varphi_i \tag{4}$$

is conveniently solvable for a complete set of bound and continuum states with eigenvalues $\epsilon_i$. These $\varphi_i$'s are restricted-Hartree–Fock(RHF)+type orbitals. A normalized zero-order determinantal wave function $\Phi_0$ can be formed out of $N$ of these single-particle states satisfying the unperturbed Schrödinger equation

$$\mathcal{H}_0 \Phi_0 = E_0 \Phi_0 \ . \tag{5}$$

The normalized eigenfunction $\Psi_0$ of the total Hamiltonian $\mathcal{H}$ could be generated from the unperturbed eigenfunction $\Phi_0$ by slowly "turning on" the perturbation "adiabatically" and using the unitary time-development operator[1,9] $U(t, t')$ defined by

$$\Psi(t) = U(t, t')\Psi(t') \ , \qquad \Psi_0 = U(0, -\infty)\Phi_0 . \tag{6}$$

The expectation value of an operator $O$ over the actual wave function $\Psi_0$ can then be shown after some manipulation to be

$$\langle O\rangle = \langle\Psi_0 | O | \Psi_0\rangle = \langle\Phi_0 | U(\infty, 0)OU(0, -\infty) | \Phi_0\rangle_L \ , \tag{7}$$

where $L$ indicates that only linked diagrams are to be considered. The relationship of this type of procedure involving linked expectation-value diagrams and the alternate one of using linked wave-function diagrams has been discussed in Ref. 7. On using the perturbation expansion

$$U(t, t_0) = \sum_{p=0}^{\infty} U_p(t, t_0) \ ,$$

where

$$U_p(t, t_0) = (-i)^p \int_{t_0}^{t} dt_1 \int_{t_0}^{t_1} dt_2 \cdots \int_{t_0}^{t_{p-1}} dt_p \times \mathcal{H}_I'(t_1)\mathcal{H}_I'(t_2)\cdots\mathcal{H}_I'(t_p) \ , \tag{8}$$

and substituting in Eq. (7), the latter can be re-expressed in the alternate form

$$\langle O\rangle = \sum_n \sum_m \langle \Phi_0 | [\mathcal{H}'(E_0 - \mathcal{H}_0)^{-1}]^n \times O[(E_0 - \mathcal{H}_0)^{-1}\mathcal{H}']^m | \Phi_0\rangle_L \ , \tag{9}$$

more amenable for diagrammatic expression.

### B. Basis Set

As is well known from the literature on the LCMBPT procedure, for the evaluation of the diagrams associated with the perturbation expansion in Eq. (9), one needs a complete set of basis states which are eigenfunctions of the zero order of Hamiltonian $\mathcal{H}_0$.

For the single-particle potential associated with the $\mathcal{H}_0$, we have chosen the $V^{N-1}$-type potential with a view towards quick convergence of the perturbation series.[2–6,10] The $V^{N-1}$ potential generates a complete, orthonormal set of infinite number of bound and continuum states. The bound-state ($\epsilon < 0$) wave functions can be separated into radial, angular, and spin components, characterized by the orbital quantum numbers $n$, $l$, and $m$ and spin quantum numbers $\sigma$ and $m_\sigma$, and can be written

$$\varphi = [P(nl; r)/r]\, Y_l^m(\theta, \phi)\chi_\sigma(m_\sigma) \ . \tag{10}$$

The form of the continuum state ($\epsilon_k = \frac{1}{2}k^2$) partial-wave wave functions is the same except that the principal quantum number $n$ is replaced by the continuously varying parameter $k$. The $s$ states are generated in the field of $1s^2 2p$ and $l > 0$ states in the field of $1s^2 2s$. In both the cases, a full exchange with the core $2s$ and $2p$ is taken. The radial equation for $l = 0$ state is

$$\left(\frac{d^2}{dr^2} + \frac{2N}{r} - \frac{1}{r}[4Y_0(1s^0, 1s^0; r) + 2Y_0(2p^0, 2p^0; r)] - 2\epsilon_{ns}\right) P(ns; r) + \frac{2}{r}[Y_0(1s^0, ns; r)P(1s^0; r) + \tfrac{1}{3}Y_1(2p^0, ns; r)P(2p^0; r)] = 0 \ , \tag{11}$$

and for $l > 0$ state,

$$\left(\frac{d^2}{dr^2} + \frac{2N}{r} - \frac{1}{r}[4Y_0(1s^0, 1s^0; r) + 2Y_0(2s^0, 2s^0; r)] - 2\epsilon_{nl}\right) P(nl; r) + \frac{2}{(2l+1)r}[Y_l(1s^0, nl; r)P(1s^0; r) + Y_l(2s^0, nl; r)P(2s^0; r) = 0 \ , \tag{12}$$

where

$$Y_k(nl, n'l'; r) = r \int_0^\infty \frac{r_<^k}{r_>^{k+1}} P(nl; r')P(n'l'; r')dr' .$$

The $P(nl; r)$ for bound states are normalized to 1. The continuum-state wave functions are normalized in such a way that the asymptotic solution at large distance $r_0$ has the form

$$P(kl; r) \to (2/r_0)^{1/2} \sin[kr + \delta_l + (1/k)\ln(2kr) - \tfrac{1}{2}l\pi].$$

In keeping with this in carrying out summation over continuum states, the relation[11]

$$\sum_k = \frac{2}{\pi} \int_0^\infty dk$$

has to be used.

In order to solve Eqs. (11) and (12), one has to make a choice of the $1s^0$, $2s^0$, and $2p^0$ wave functions in obtaining the $Y_k$'s. In case RHF wave functions for these states are available, one could make use of those in $Y_k$'s. But, since no accurate RHF wave functions were available for the $^3P$ state of beryllium, the following procedure was adopted in solving the basis set equations (11) and (12). We started with the $1s$ and $2s$ wave functions for the $1s^2 2s^2$ state from Clementi's table.[12] With this choice, the $2s$ and $2p$ wave functions were obtained from solutions of Eqs. (11) and (12) and then, the process was repeated until the $2s$ and $2p$ wave functions had converged as they should with the choice made for the $V^{N-1}$ potential. Only a few cycles (about three) were needed for the convergence.

### C. Formalism for Hyperfine-Interaction Constant

The Hamiltonian terms corresponding to the Fermi-contact, dipole-dipole and magnetic-orbital interactions can be written

$$\mathcal{H}_c' = \frac{16\pi}{3} \frac{\mu_B \mu_N}{I a_B^3} \vec{I} \cdot \sum_{i=1}^N \vec{s}_i \delta(\vec{r}_i) , \tag{13}$$

$$\mathcal{H}_d' = 2 \frac{\mu_B \mu_N}{I a_B^3} \vec{I} \cdot \sum_{i=1}^N \left( \frac{3(\vec{s}_i \cdot \vec{r}_i)\vec{r}_i}{r_i^5} - \frac{\vec{s}_i}{r_i^3} \right) \tag{14}$$

$$\mathcal{H}_o' = 2 \frac{\mu_B \mu_N}{I a_B^3} \vec{I} \cdot \sum_{i=1}^N \frac{\vec{l}_i}{r_i^3} \tag{15}$$

In the experimental determination of atomic hfs, one uses the spin Hamiltonian

$$\mathcal{H}' = A_J \vec{I} \cdot \vec{J} , \tag{16}$$

where $J$ is the total electronic angular momentum and $A_J$ is the magnetic-hyperfine-coupling constant. The individual hyperfine-coupling constants in Hertz corresponding to the three types of interactions mentioned above can be written in terms of expectation values of the three hyperfine Hamiltonian terms

$$\begin{aligned}
A_c &= \left( \frac{16\pi}{3} \frac{\mu_B \mu_N}{I M_J a_B^3 h} \right) \left\langle \Psi(J, M_J) \middle| \sum_{i=1}^N s_{z_i} \delta(\vec{r}_i) \middle| \Psi(J, M_J) \right\rangle , \\
A_d &= \left( \frac{2\mu_B \mu_N}{I M_J a_B^3 h} \right) \left\langle \Psi(J, M_J) \middle| \left( \sum_{i=1}^N \frac{3\vec{s}_i \cdot \vec{r}_i}{r_i^5} z_i - \frac{s_{z_i}}{r_i^3} \right) \middle| \Psi(J, M_J) \right\rangle , \\
A_o &= \left( \frac{2\mu_B \mu_N}{I M_J a_B^3 h} \right) \left\langle \Psi(J, M_J) \middle| \sum_{i=1}^N \frac{l_{z_i}}{r_i^3} \middle| \Psi(J, M_J) \right\rangle .
\end{aligned} \tag{17}$$

The evaluation of $A_c$, $A_d$, and $A_o$ thus involves calculation of the expectation values in the three equations of (17) in terms of perturbation diagrams. For diagrammatic notation, we represent the contact, dipolar, and orbital operators, (for $3P_2$ state with $M_J = 2$) $2s_z\delta(\vec{r})$, $s_z(3z^2 - r^2)/r^5$, and $l_z/r^3$ as wiggly lines followed by letters $c$, $d$ and $o$, respectively. To obtain the contributions to $A_c$, $A_d$, and $A_b$ in Hertz from the individual diagrams which are evaluated in units of $a_B^{-3}$, one has to apply the multiplying factor

$$K_c = \tfrac{8}{3}\pi \mu_B \mu_N / I M_J a_B^3 h \tag{18}$$

for the contact case and the factor

$$K_d = 2\mu_B \mu_N / I M_J a_B^3 h \tag{19}$$

for the dipolar and orbital cases.

### D. Description of Hyperfine Diagrams

With the contact, dipolar, and orbital operators introduced in the place of $O$ in Eq. (7), the different terms in the perturbation series can be obtained by assigning different integral values (including zero) to $m$ and $n$. A particular term in this series can be represented by a group of Feynmann-like diagrams drawn according to rules described in the LCMBPT literature.[1-7,10] As usual, in the diagrams in Figs. 1 through 6, the downward lines correspond to holes, and the upward to particles, while the horizontal dotted lines correspond to electron-electron interactions. The diagrams corresponding to $m$ and $n$ orders in Eq. (9) are referred to as $(m, n)$ diagrams. For example, the $m = 0$, $n = 1$ contact diagrams in Figs. 1(a) and 1(b) are

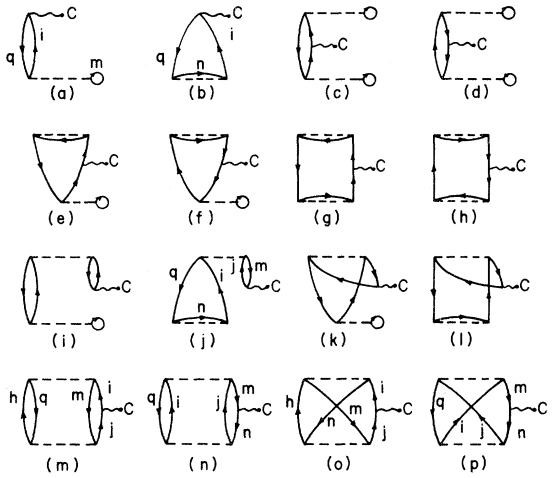

FIG. 1. (0,1) and (1,1) contact diagrams.

referred to as (0, 1) diagrams. Similarly, the rest of the diagrams in Fig. 1 are referred to as (1, 1) and those in Fig. 2 as (0, 2) diagrams. Because of the Hermiticity of the operators involved in Eqs. (17), the contributions from $(m,n)$ and $(n,m)$ diagrams are equal. In presenting the diagrams proper care has been taken to include cancellations among diagrams associated with spin and between the potential terms and the electron-electron interactions involving unexcited occupied states.

We consider first the contact diagrams. For these diagrams, it is the $c$ vertex that has to be used and, in view of its $\delta$-function character, it has to be attached only to $s$-hole and particle states.

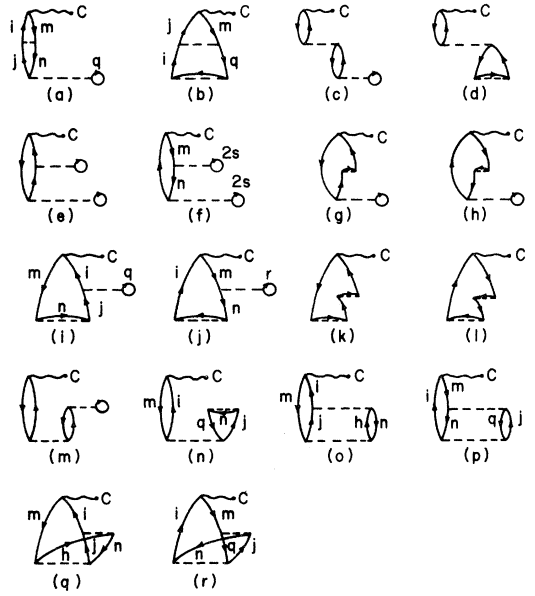

FIG. 2. (0,2) contact diagrams.

In Fig. 1, we present the (0, 1) and (1, 1) contact hyperfine diagrams. Diagram 1(a) represents the influence of the asymmetry of the phase space available for excitation to the $1s$ spin-up and spin-down electrons because the $2s$ up-spin state is occupied, while the $2s$ down state is vacant. This diagram, in keeping with the earlier literature in the field, will be referred to as a phase-space diagram. Diagram 1(b) represents the exchange core-polarization (ECP) effect of the spin-up valence electrons ($2s$, $2p$) on the $1s$ core electrons. The diagrams shown in 1(c)–1(h) represent single-excitation effects in each of which, the contact-hyperfine operator appears between two first-order (single-excitation) wave functions. In Figs. 1(i) and 1(j) are shown the result of combinations of correlation, phase-space, and ECP effects which may, for brevity, be together referred to as core-polarization effects. Figures 1(k) and 1(l) are the exchange counterparts of 1(i) and 1(j). The rest of the (1, 1) diagrams [1(m) through 1(p)], represent purely correlation effects. The (0, 2) contact hyperfine diagrams are shown in Fig. 2. Diagrams 2(a)–2(l) can be obtained from diagrams 1(a) and 1(b) by attaching one more order of electron-electron interaction to hole and particle lines. These diagrams represent an interplay between core-polarization and consistency effects, whereas Figs. 2(m) and 2(n) represent interaction between correlation and core-polarization effects. The last four diagrams, 2(o)–2(r) in Fig. 2, show mutual polarization effects in the second-order wave functions.

The dipole and orbital diagrams shown in Figs. 3–5 represent similar physical effects as in the contact case, but with different hyperfine operators. Equation (17) shows that dipole operator has the form $Y_2^0$ and so, this operator by the usual angular momentum vector addition rules connects states

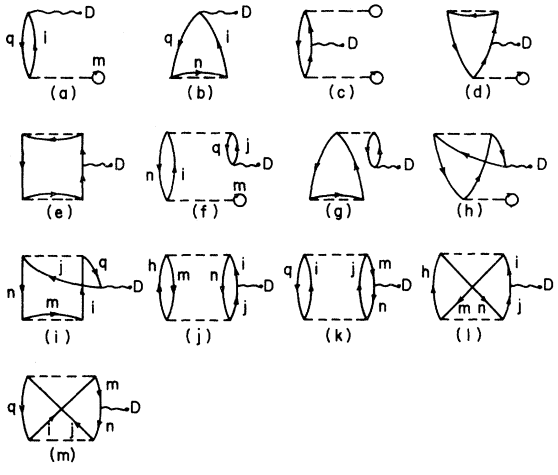

FIG. 3. (0,1) and (1,1) dipole diagrams.

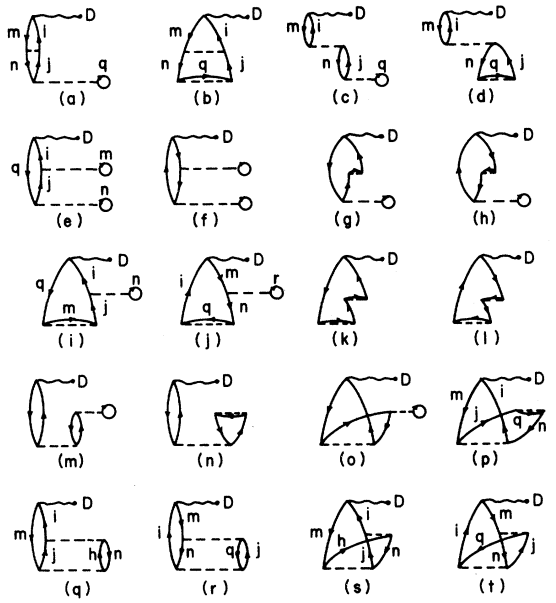

FIG. 4. (0, 2) dipole diagrams.

differing in $l$ by zero or two, except that the former is not allowed for $s$ states. For example, in diagram 3(f), one can have for $q$ a $2s$ state and for $j$ a $d$-particle state, or have $q$ as $2p$ and $j$ as $p$. The orbital operator in Eq. (17) involves $l_z$ and hence, connects non-$s$ states of same $l$. Figure 6 shows some important third-order contact diagrams which represent the combined effect of ECP and mutual polarization effects.

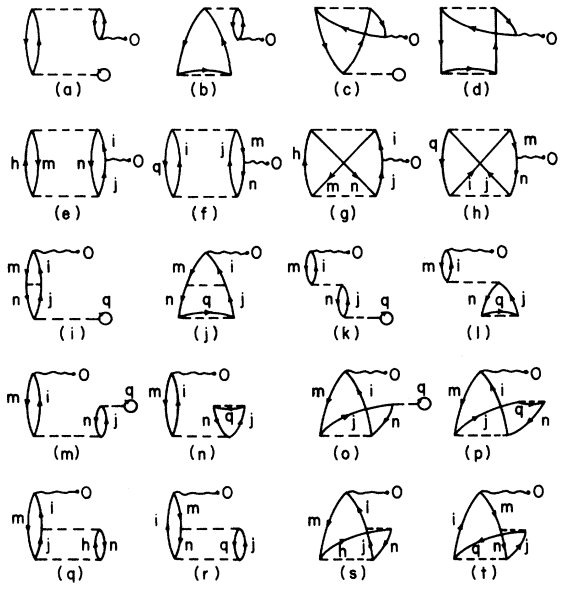

FIG. 5. Orbital diagrams.

TABLE I. Contributions to Fig. 2(o) from various angular momentum states with $m=2s^+$, $n=1s^+$.

| $j$ | $h$ | Contribution in MHz |
|---|---|---|
| $s$ | $s$ | −1.100 |
| $p$ | $p$ | −0.795 |
| $d$ | $d$ | −0.150 |
| $f$ | $f$ | −0.038 |

## III. RESULTS OF CALCULATION

As mentioned earlier, the evaluation of diagrams requires a complete set of basis functions. The nature of the convergence with respect to $l$ observed in the present work and in earlier work on atomic hyperfine interaction indicated that it was sufficient to use up to $f$ states in evaluating the diagrams. To demonstrate the nature of this convergence, contributions from various angular momentum states to a typical diagram, namely, that in Fig. 2(o) is given in Table I. For particle states of particular $l$, we include bound states up to principal quantum number $n=10$ while, the $k$ values that characterize the continuum states were chosen appropriately to apply a 12-point Gauss–Laguerre integration technique for $k$ space. These bound- and continuum-state wave functions were obtained by solving Eqs. (11) and (12) using numerical procedures discussed elsewhere.[4,13,14]

We shall now consider the results of calculation for the individual hyperfine interactions, contact, dipolar, and orbital, separately. The conversion factors $K_c$ and $K_d$ defined in Eq. (18) and used to convert the values of the diagrams in atomic units ($a_B^{-3}$) to megahertz were calculated[15] to be −156.84 and −37.443, respectively.

In Tables II through VIII, giving values of various diagrams, superscripts ± are used to indicate

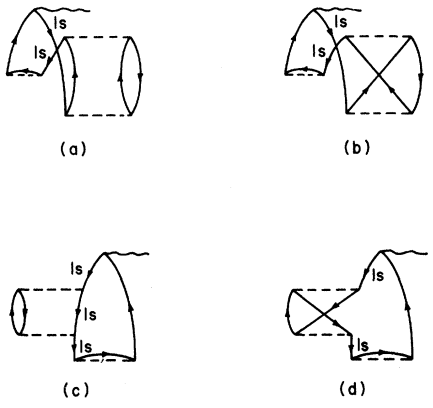

FIG. 6. Some important third-order contact diagrams.

TABLE II. Contributions from (0, 1) diagrams shown in Figs. 1(a)–1(b).

| Diagram | Excitation | Contribution in MHz |
|---|---|---|
| 1(a) | $q=1s^-$ $m=2s$ $i=2s^-$ | −1.417 |
| 1(b) | $q=1s^+$ $n=2s$ $i=s^+$ | −16.572 |
| | $q=1s^-$ $n=2p$ $i=s^-$ | 6.545 |
| Total | | −11.444 |

the spins associated with the corresponding one-particle states. When states $2s$ and $2p$ appear without any superscript, the state is either a spin-up state or the corresponding spin-independent states used in the construction of the $V^{N-1}$ potential. We use this convention because, with our choice of $V^{N-1}$ potential, there is no difference between the $2s$, $2p$ states used in calculating the potential and the corresponding spin-up states.

### A. Fermi-Contact Interaction

There is a direct RHF contribution from the unpaired $2s$ electron which gives −98.579 MHz. In Tables II–V, for brevity, we have listed individually only the values of those diagrams which contribute more than 0.25 MHz. For the rest of the diagrams, only the net sum is indicated. In Table II, we present the contributions from (0, 1) diagrams shown in Figs. 1 (a) and 1(b). The total contribution from these first-order core-polarization diagrams is found to be −11.444 MHz which is about 11.5% of the direct RHF contribution.

The core-polarization contribution is composed of −16.572 MHz due to the ECP effect of the valence $2s$ state on the $1s^2$ core, 6.545 MHz from the ECP effect of the valence $2p$ state, and −1.417 MHz from the phase-space diagram in Fig. 1 (a) associated with the influence of the $2s$ state. Thus the net core polarization of −11.444 MHz is composed of −17.989 MHz from the influence of the $2s$ state and 6.545 MHz from the $2p$ state. The greater relative contribution from the $2s$ state, opposite in sign to that from the $2p$ state is in keeping with the trend observed for the ground $(^2S)^2$ and excited $(^2P)$ states[6] of lithium, the overall difference in sign from the lithium results being a consequence of the opposite signs of the nuclear magnetic moments of $Li^7$ and $Be^9$.

The contributions from (1, 1) diagrams are presented in Table III. The diagrams in Figs. 1(c)–1(h) all involve single-particle excitations, since they all have only one particle line at any time. These diagrams are all seen to contain one or two $1s$-hole lines. Because of the relatively large negative energy of the $1s$ state, the energy denominators involved in these diagrams are substantial and hence, their contributions are small, as shown in the second line of Table III. The diagrams 1(i)–1(l) appear to involve two particles excited simultaneously at certain times. However, it has been shown earlier that the influence of these diagrams can be characterized as a one-electron consistency effect, representing the influence of the self-consistent interaction between the electrons on the core-polarization effect. The contributions from these diagrams are, therefore, listed under the heading consistency in Table III. The preponderance of the combined contributions of diagrams 1(j) through 1(l) compared to 1(i) is a consequence of the greater importance of ECP effects represented by 1 (b) as compared to the phase-space contribution in diagram 1(a).[16] The rest of the (1, 1) diagrams [1(m)–1(p)] represent correlation effects having two particles excited at any time. Their contributions are listed in Table III, the major contributions from this class arising from the $2s$-$2p$ correlation effect as expected. The contributions from the diagrams 1(m) and 1(n) are cancelled substantially by their exchange counterparts 1(o) and 1(p), respectively. The total contribution from the (1, 1) diagrams was found to be 0.281 MHz, which is only 0.3% of the direct RHF contribution and of opposite sign.

Tables IV and V contain the contributions from the various (0, 2) diagrams of Fig. 2. In Table IV, we present the values of diagrams 2(a)–2(n). The major contributions from this class come from second-order diagrams 2(a), 2(b), 2(i), 2(j), and 2(n), which are topologically related to the core-polarization diagrams. Due to relatively important contributions from these diagrams, as compared to others of second-order, some third-order diagrams which are extensions of these diagrams

TABLE III. Contributions from (1,1) diagrams shown in Figs. 1(c)–1(p).

| Diagram | Excitation | Contribution in MHz |
|---|---|---|
| | Single excitation | |
| 1(c)–1(h) | | 0.054 |
| | Consistency | |
| 1(j) | $q=1s^+$ $m=1s^-$ $n=2s$ | −0.479 |
| | $q=1s^-$ $m=1s^+$ $n=2p$ | 0.269 |
| Other consistency diagrams | | −0.052 |
| | Correlation | |
| 1(m) | $q=1s^\pm$ $m=2s^+$ $i=s^+$ $j=s^+$ | −0.394 |
| | $q=2p^+$ $m=2s^+$ $i=s^+$ $j=s^+$ | −0.776 |
| 1(n) | $q=2p^+$ $m=n=2s^+$ | 3.981 |
| | $q=2p^+$ $m=1s^+$ $n=2s^+$ | −0.521 |
| 1(o) | $m=2s^+$ $n=1s^+$ $h=s^+$ $i=s^+$ $j=s^+$ | 0.365 |
| | $m=2s^+$ $n=2p^+$ $h=p^+$ $i=s^+$ $j=s^+$ | 0.504 |
| 1(p) | $q=2p^+$ $m=1s^+$ $n=2s^+$ | 0.355 |
| | $q=2p^+$ $m=2s^+$ $n=2s^+$ | −2.867 |
| Other correlation diagrams | | −0.158 |
| Total | | 0.281 |

TABLE IV. Contributions from (0,2) diagrams shown in Figs. 2(a)–2(n).

| Diagram | Excitation | | | | Contribution in MHz |
|---|---|---|---|---|---|
| 2(a) | $m=n=1s^-$ | $q=2s$ | | | −0.512 |
| 2(b) | $m=1s^+$ | $q=1s^+$ | $n=2s$ | $i=s^+$ | −2.761 |
| | $m=1s^-$ | $q=1s^-$ | $n=2p$ | $i=s^+$ | 1.552 |
| 2(i) | $m=1s^-$ | $q=2s$ | $n=2p$ | $j=s^-$ | −0.796 |
| 2(j) | $m=n=1s^+$ | $q=2s$ | $r=2s$ | | −0.780 |
| | $m=n=1s^-$ | $q=2p$ | $r=2s$ | | 0.541 |
| 2(n) | $m=1s^-$ | $q=1s^+$ | $n=2s$ | | −0.383 |
| Other diagrams | | | | | 0.013 |
| Total | | | | | −3.126 |

will be considered. Table V shows values of diagrams 2(o)–2(r) which represent correlation effects that may be characterized as mutual polarization of pairs of orbitals by each other. The major contributions in this case arise from the correlation of $2s$ and $2p$ and of $1s$ and $2s$, the former being the leading one. The total contribution from (0, 2) diagrams was found to be − 5.445 MHz, that is about 5.5% of the direct RHF contribution.

In considering third- and higher-order diagrams, it is convenient for purposes of discussion to separate these diagrams into two categories. The first category involves corrections to hole and particle states involved in lower-order diagrams due to the use of a $V^{N-1}$ potential. This category, often referred to as ladder diagrams, is exemplified by taking higher-order counterparts of diagrams 2(f) and 2(j) with $m=n=1s$ and with another $2s$ bubble attached to the hole side. Thus, 2(f) and its next-higher-order counterpart represent the first two of the set of hole-hole ladder diagrams associated with 1(a). Similarly 2(j) and its next-higher-order counterpart represent the first two of the ladder diagrams associated with the ECP diagram 1(b) with $n=2s$ or $2p$. These ladder corrections are carried out to all orders by replacing the $V^{N-1}$ $1s$ energy in the energy denominators of diagrams 1(a) and 1(b) by the Hartree–Fock $1s$ energy. Similarly, diagram 2(b) with $m=q=1s$ and its higher-order counterpart involving another horizontal interaction line represent the first two of the hole-particle ladder diagrams associated with the ECP diagram 1(b). These hole-particle ladder corrections cannot be summed analytically as in the case of hole-hole ladders. Instead, as is usually the practice, the geometric series nature was tested by taking ratios of successive orders and checking for their constancy. The influence of these ladder corrections were nearly equal and opposite for the $2s$ and $2p$ core-polarization diagrams leading to a total correction of − 0.062 MHz.

The hole-hole and hole-particle ladder corrections were applied to all orders, since they represent corrections to the one-electron energies from those appropriate for the $V^{N-1}$ potential chosen to the proper self-consistent ones for the various hole states.

We feel however, that selective summations to all orders should not be applied to a few of the other classes of higher-order diagrams, unless one can do this for all important third-order diagrams of comparable magnitude. This was not an important consideration here however, because the third-order diagrams besides the ladder types already considered were quite small. A few typical classes of third-order diagrams that we have considered are presented in Figs. 6(a)–6(d), of which Figs. 6(a) and 6(b) are referred to as renormalization diagrams. The contributions from these diagrams are, respectively, 0.045 and − 0.020 MHz.

The final result of our calculation for the contact contribution to the hyperfine constant including RHF, (0, 1), (1, 1), and (0, 2) contributions, together with the hole-hole and hole-particle ladder corrections and third-order diagrams in Fig. 6 is − 115.22 MHz.

### B. Dipole-Dipole Interaction

The dipole-dipole operator is also spin dependent like the contact operator so that there would again be a cancellation between the lowest-order contributions from two $1s$ electrons. However, in view of the tensor nature of the dipole-dipole interaction, the individual contribution from each $1s$ electron also vanishes. The direct RHF contribution, therefore, arises only from the unpaired $2p$ elec-

TABLE V. Contributions from (0,2) diagrams shown in Figs. 2(o)–2(r).

| Diagram | Excitation | | | | Contribution in MHz |
|---|---|---|---|---|---|
| 2(o) | $m=1s^{\mp}$ | $n=1s^{\pm}$ | | | 0.731 |
| | $m=2s^+$ | $n=1s^{\pm}$ | | | −4.629 |
| | $m=2s^+$ | $n=2p^+$ | | | −3.475 |
| 2(p) | $q=1s^-$ | $m=1s^+$ | $n=2s^+$ | $i=s^+$ | 0.397 |
| | $q=1s^-$ | $m=2s^+$ | $n=1s^+$ | $i=s^+$ | 0.916 |
| | $q=1s^+$ | $m=n=1s^-$ | | $i=2s^-$ | −0.969 |
| | $q=1s^-$ | $m=n=1s^+$ | | $j=2s^-$ | 0.820 |
| | $q=2s^+$ | $m=n=1s^-$ | | $i=2s^-$ | −0.369 |
| | $q=m=1s^+$ | $n=2s^+$ | | | 0.353 |
| | $q=m=2s^+$ | $n=2p^+$ | | | 0.256 |
| | $m=n=2s^+$ | $q=2p^+$ | | | 2.722 |
| 2(q) | $m=2s^+$ | $n=2p^+$ | | | 1.153 |
| | $m=2s^+$ | $n=1s^+$ | | | 1.814 |
| | $m=1s^+$ | $n=2s^+$ | | | 0.939 |
| | $m=1s^+$ | $n=2p^+$ | | | 0.536 |
| 2(r) | $m=n=1s^+$ | $q=2s^+$ | | | −0.360 |
| | $m=n=2s^+$ | $q=2p^+$ | | | −0.668 |
| | $m=q=1s^+$ | $n=2s^+$ | | | −0.992 |
| | $m=q=2s^+$ | $n=1s^+$ | | | −0.989 |
| | $m=q=1s^+$ | $n=2p^+$ | | | 0.382 |
| Other diagrams | | | | | 0.185 |
| Total | | | | | −2.319 |

TABLE VI. Contributions from (0,1) and (1,1) diagrams shown in Fig. 3.

| Diagram | Excitation | | Contribution in MHz |
|---|---|---|---|
| 3(a) | $q=2s^+$ | $m=2p$ | −0.0661 |
| 3(b) | $q=1s^+$ | $n=2p$ | 0.1086 |
| | $q=2s^+$ | $n=2p$ | 0.1331 |
| Total from (0,1) diagrams | | | 0.1756 |
| 3(j) | $m=2s^+$ | $n=2p^+$ | 0.0498 |
| | $m=2p^+$ | $n=2s^+$ | 0.0061 |
| 3(k) | $m=n=2p^+$ | $q=2s^+$ | −0.0892 |
| 3(l) | $m=2s^+$ | $n=2p^+$ | −0.0292 |
| 3(m) | $m=n=2p^+$ | $q=2s^+$ | 0.0643 |
| Other diagrams | | | −0.0075 |
| Total from (1,1) diagrams | | | −0.0059 |

tron and is 2.208 MHz. This is the major contribution from the dipole-dipole diagrams, since all the higher-order diagrams are an order of magnitude smaller than the direct one. In Tables VI and VII, we present the values of those diagrams which contribute more than 0.003 MHz. Table VI lists the contributions from the (0, 1) and (1, 1) diagrams shown in Fig. 3. The first three lines list the contributions from the three (0, 1) diagrams which, taken together, contribute to 0.1756 MHz. This is about 8% of the direct RHF contribution. The one-electron-type diagrams [Fig. 3(c)–3(e)] and consistency diagrams [Fig. 3(f)–3(i)] do not make appreciable contributions. The contributions from correlation diagrams [Fig. 3(j)–3(m)] are mainly due to $2s$-$2p$ correlation. The total contribution from (1, 1) diagrams is −0.0057 MHz, which is only about 0.25% of the direct RHF contribution. In Table VII, the contributions from the (0, 2) diagrams of Fig. 4 are listed. Among the one-electron-type diagrams, the contributions from Figs. 4(b) and 4(i) are relatively larger. Both these diagrams involve $2s$ and $2p$ hole states which are expected to interact strongly. However, these two diagrams have opposite sign and thus nearly cancel each other. Similarly, the next two important one-electron (0, 2) diagrams in Figs. 4(a) and 4(e) also nearly cancel. Consequently, the net contributions from all the diagrams in Figs. 4(a)–4(p) are very small. The relatively small sizes of these diagrams and their close cancellations indicate that in this case, the laddering for the (0, 1) diagrams is even less significant than for the contact interaction.

The correlation diagrams 4(q)–4(t) of order (0, 2) individually contribute very little as shown in the table. The appreciable ones among these are the diagrams which involve $2s$-$2p$ correlation. The total contribution from (0, 2) diagrams is −0.0523 MHz, which is only about 2.4% of the direct RHF contribution. The net contribution to the hyperfine constant from the dipole-dipole interaction is then found to be 2.4302 MHz.

### C. Magnetic-Orbital Interaction

The magnetic-orbital operator has the same radial form as the dipole-dipole case. The angular part here is different from the dipole-dipole case and there is no spin dependence involved. There are no (0, 1) diagrams in this case. The values of most of the orbital-hyperfine diagrams of order (1, 1) and (0, 2) shown in Fig. 5 can be obtained from the corresponding dipole-dipole diagrams by multiplication with appropriate angular factors. However, in view of the absence of spin dependence, some new diagrams appear in the orbital case, which had cancelled out for the dipolar interaction through the spin dependence of the latter. The values of only those orbital diagrams which are larger in size than 0.003 MHz are listed in Table VIII. Summarizing, the direct RHF contribution from the magnetic-orbital interaction is −11.0381 MHz. There are no (0, 1) diagrams. The contribution from (1, 1) and (0, 2) diagrams are −0.0650 and +0.3091 MHz, respectively, adding up to a total magnetic-orbital contribution of

TABLE VII. Contributions from (0,2) diagrams shown in Fig. 4.

| Diagram | Excitation | | | | Contribution in MHz |
|---|---|---|---|---|---|
| 4(a) | $m=n=2s^+$ | $q=2p$ | $i=d^+$ | | −0.0529 |
| 4(b) | $m=n=1s^+$ | $q=2p$ | $i=d^+$ | | 0.0249 |
| | $m=n=2s^+$ | $q=2p$ | $i=d^+$ | | 0.1140 |
| | $m=1s^+$ | $n=2s^+$ | $q=2p$ | $i=d^+$ | −0.0052 |
| | $m=2p^+$ | $n=2s^+$ | $q=2p$ | $i=p^+$ | −0.0055 |
| 4(c) | $m=n=2s^+$ | $q=2p$ | | $i=d^+$ | 0.0035 |
| 4(d) | $m=n=2s^+$ | $q=2p$ | | $i=d^+$ | −0.0078 |
| | $m=2p^+$ | $n=2s^+$ | $q=2p$ | | −0.0042 |
| 4(e) | $m=n=2p$ | $q=2s^+$ | $i=d^+$ | $j=d^+$ | 0.0520 |
| 4(i) | $m=n=2p$ | $q=1s^+$ | | $j=d^+$ | −0.0139 |
| | $m=n=2p$ | $q=2s^+$ | | $j=d^+$ | −0.1120 |
| 4(j) | $m=n=1s^+$ | $q=2p$ | $r=2s$ | | 0.0050 |
| 4(p) | $m=2p^+$ | $n=2s^+$ | $q=2p$ | | 0.0053 |
| 4(q) | $m=2s^+$ | $n=2p^+$ | | | 0.0224 |
| | $m=2p^+$ | $n=1s^\pm$ | $i=p^+$ | | 0.0837 |
| | $m=2p^+$ | $n=2s^+$ | $i=p^+$ | | 0.1306 |
| 4(r) | $m=1s^+$ | $n=2p^+$ | $q=1s^\pm$ | $i=d^+$ | −0.0063 |
| | $m=2p^+$ | $n=1s^+$ | $q=1s^-$ | $i=p^+$ | −0.0073 |
| | $m=2p^+$ | $n=2s^+$ | $q=1s^\pm$ | $i=p^+$ | −0.0035 |
| | $m=2p^+$ | $n=2s^+$ | $q=2p^+$ | $i=p^+$ | −0.0079 |
| | $m=n=2p^+$ | | $q=2s^+$ | $i=p^+$ | −0.0728 |
| 4(s) | $m=1s^+$ | $n=2p^+$ | | | −0.0089 |
| | $m=2s^+$ | $n=2p^+$ | | | −0.0282 |
| | $m=2p^+$ | $n=1s^+$ | | $i=p^+$ | −0.0120 |
| | $m=2p^+$ | $n=2s^+$ | | $i=p^+$ | −0.0932 |
| 4(t) | $m=n=1s^+$ | $q=2p^+$ | | $i=d^+$ | 0.0077 |
| | $m=n=2s^+$ | $q=2p^+$ | | $i=d^+$ | 0.0035 |
| | $m=n=2p^+$ | $q=2s^+$ | | $i=p^+$ | 0.0280 |
| | $m=q=2p^+$ | $n=2s^+$ | | $i=p^+$ | 0.0100 |
| Other diagrams | | | | | 0.0033 |
| Total | | | | | −0.0523 |

TABLE VIII. Contributions from diagrams shown in Fig. 5.

| Diagram | Excitation | | | | Contribution in MHz |
|---|---|---|---|---|---|
| 5(e) | $m=1s^{\pm}$ | $n=2p^{+}$ | | | −0.0273 |
| | $m=2s^{+}$ | $n=2p^{+}$ | | | −0.2777 |
| | $m=2p^{+}$ | $n=1s^{\pm}$ | | | 0.0182 |
| | $m=2p^{+}$ | $n=2s^{+}$ | | | −0.2373 |
| 5(f) | $m=n=2p^{+}$ | $q=2s^{+}$ | | | 0.4460 |
| 5(g) | $m=2s^{+}$ | $n=2p^{+}$ | | | 0.3311 |
| 5(h) | $m=n=2p^{+}$ | $q=2s^{+}$ | | | −0.3215 |
| Other (1,1) diagrams | | | | | 0.0035 |
| Total from (1,1) diagrams | | | | | −0.0650 |
| 5(i) | $m=2p^{+}$ | $n=1s^{+}$ | $q=2p$ | $i=p^{+}$ | −0.0047 |
| | $m=2p^{+}$ | $n=1s^{+}$ | $q=2s$ | $i=p^{+}$ | −0.0034 |
| 5(j) | $m=2p^{+}$ | $n=1s^{+}$ | $q=2p$ | $i=p^{+}$ | −0.0052 |
| | $m=2p^{+}$ | $n=1s^{+}$ | $q=2s$ | $i=p^{+}$ | 0.0045 |
| | $m=2p^{+}$ | $n=2s^{+}$ | $q=2p$ | $i=p^{+}$ | 0.0274 |
| 5(k) | $m=2p^{+}$ | $n=1s^{\pm}$ | $q=2s$ | $i=p^{+}$ | −0.0060 |
| | $m=2p^{+}$ | $n=2s^{+}$ | $q=2p$ | $i=p^{+}$ | −0.0053 |
| 5(l) | $m=2p^{+}$ | $n=1s^{+}$ | $q=2s$ | $i=p^{+}$ | 0.0033 |
| | $m=2p^{+}$ | $n=1s^{+}$ | $q=2p$ | $i=p^{+}$ | 0.0046 |
| | $m=2p^{+}$ | $n=2s^{+}$ | $q=2p$ | $i=p^{+}$ | 0.0055 |
| 5(m) | $m=2p^{+}$ | $n=1s^{\pm}$ | $q=2s$ | $i=p^{+}$ | −0.0050 |
| | $m=2p^{+}$ | $n=2s^{+}$ | $q=2p$ | $i=p^{+}$ | −0.0044 |
| 5(n) | $m=2p^{+}$ | $n=1s^{+}$ | $q=2s$ | $i=p^{+}$ | 0.0069 |
| | $m=2p^{+}$ | $n=1s^{\pm}$ | $q=2p$ | $i=p^{+}$ | 0.0029 |
| | $m=2p$ | $n=2s^{+}$ | $q=2p$ | $i=p$ | 0.0091 |
| 5(o) | $m=2p^{+}$ | $n=1s^{+}$ | $q=2s$ | $i=p^{+}$ | −0.0030 |
| | $m=2p^{+}$ | $n=2s^{+}$ | $q=2p$ | $i=p^{+}$ | 0.0111 |
| 5(p) | $m=2p^{+}$ | $n=1s^{+}$ | $q=2s$ | $i=p^{+}$ | 0.0040 |
| | $m=2p^{+}$ | $n=2s^{+}$ | $q=2p$ | $i=p^{+}$ | −0.0242 |
| 5(q) | $m=2p^{+}$ | $n=1s^{\pm}$ | | $i=p^{+}$ | −0.4185 |
| | $m=2p^{+}$ | $n=2s^{+}$ | | $i=p^{+}$ | −0.6530 |
| 5(r) | $m=2p^{+}$ | $n=1s^{+}$ | $q=1s^{-}$ | $i=p^{+}$ | 0.0365 |
| | $m=2p^{+}$ | $n=1s^{+}$ | $q=2s^{+}$ | $i=p^{+}$ | 0.0030 |
| | $m=2p^{+}$ | $n=2s^{+}$ | $q=1s^{\pm}$ | $i=p^{+}$ | 0.0225 |
| | $m=2p^{+}$ | $n=2s^{+}$ | $q=2p^{+}$ | $i=p^{+}$ | 0.0395 |
| | $m=n=2p^{+}$ | | $q=2s^{+}$ | $i=p^{+}$ | 0.3635 |
| 5(s) | $m=2p^{+}$ | $n=1s^{+}$ | | $i=p^{+}$ | 0.0600 |
| | $m=2p^{+}$ | $n=2s^{+}$ | | $i=p^{+}$ | 0.4660 |
| 5(f) | $m=n=2p^{+}$ | | $q=2s^{+}$ | $i=p^{+}$ | −0.1400 |
| | $m=q=2p^{+}$ | | $n=2s^{+}$ | $i=p^{+}$ | −0.0499 |
| | $m=2p^{+}$ | $n=1s^{+}$ | $q=2s^{+}$ | $i=p^{+}$ | −0.0043 |
| Other diagrams | | | | | −0.0525 |
| Total from (0,2) diagrams | | | | | −0.3091 |

−11.4122 MHz.

The total contributions from the contact, dipole-dipole, and magnetic-orbital interactions that we have obtained are presented in Table IX. The net calculated contribution to $A$ is found to be −124.206 MHz. The accuracy of our results and comparison with experiment are considered in the Sec. IV.

## IV. DISCUSSION AND CONCLUSION

The main feature of the results in Table IX is the good convergence of the results in terms of various orders of perturbation. The convergence of the contact contribution is really better than it appears from Table IX, since a substantial part of the (0, 2) contribution really refers to ladder corrections to (0, 1). On regrouping these results, the (0, 1) contribution, including ladder contribution, comes out as −14.354 MHz while the (0, 2) contribution reduces to −2.406 MHz. This situation is in marked contrast to the situations for the ground states of the rest of the elements of the second period (excluding lithium), where one has two paired $s$ shells, $2s$ and $1s$ whose core polarizations cancel strongly, making the (0, 1) contribution weak and thereby enhancing the relative importance of the higher orders. The nature of the contact interaction in the present case is closer to lithium-atom ground state with $2s$ giving a substantial zero-order contribution. As compared to lithium, the core-polarization effect is somewhat weaker relative to the zero-order contribution, because of some cancellation between the core-polarization effects of $2s$ and $2p$ electrons on the $1s$ shell, as seen from Table II. As regards the correlation contribution, the major effect arises from the diagrams 2(o)–2(r) as in the case of lithium and order alkali atoms. These diagrams represent the effects of the instantaneous polarization of the unpaired $2s$ orbital by the $1s$ core electrons as in lithium and in the present case by the $2p$ electron. Due to substantial cancellations among the four diagrams 2(o)–2(r), the net influence of $2s$-$2p$ correlations is reduced substantially, even though, as can be seen from Table V, the individual contributions from diagrams, for this correlation effect, are substantial. The relative importance of the correlation between the $1s^2$ and $2s$ orbital (relative to the zero-order contribution) as described by diagrams 2(o)–2(r) is somewhat less compared to lithium atom, mainly due to the weaker polarizability of the $2s$ orbital in beryllium.

Regarding the orbital and dipolar contributions, the convergence of the various orders is seen from Table IX to be about as good as for the contact interaction. It is interesting to compare the relative contributions from various orders with those for the $^2P$ excited state of lithium. The ratio of the (0, 1) and (0, 0) contributions to $A_d$ is significantly larger than in the case of lithium-atom $^2P$ state. The reason for this can be seen from Table

TABLE IX. Contributions from each order to the three types of magnetic hyperfine interaction (in MHz).

| Order | $A_c$ | $A_d$ | $A_o$ |
|---|---|---|---|
| (0,0) | −98.579 | 2.208 | −11.038 |
| (0,1) | −11.444 | 0.176 | 0.000 |
| (1,1) | 0.281 | −0.006 | −0.065 |
| (0,2) | −5.445 | −0.052 | −0.309 |
| Higher than (0,2) | −0.037 | ... | ... |
| Total | −115.224 | 2.430 | −11.412 |

TABLE X. One- and many-electron separation of the hyperfine constants (in MHz).

| Constant | Direct RHF value | One electron | Two electrons | Total |
|---|---|---|---|---|
| $A_c$ | −98.5790 | −14.8110 | −1.8340 | −115.2240 |
| $A_d+A_o$ | −8.8300 | 0.1960 | −0.3480 | −8.9820 |

VI. Thus, in addition to the $1s$-$2p$ exchange described by Fig. 3(b) which also occurs for the $^2P$ state of lithium, we now have additional contributions of the same sign from $2s$-$2p$ interactions both through diagram 3(b), as well as 3(a). The contribution from (1, 1) diagrams are comparable in importance, although in the present case, the major contribution comes from $2s$-$2p$ interaction instead of $1s$-$2p$ as in the case of lithium. The (0, 2) dipolar contributions indicate an interesting influence of the role of $2s$-$2p$ interactions. Thus, in the case of lithium $^2P$ state, the main contribution arose from the $1s$-$2p$ correlation represented by diagram 4(q). The contribution from the comparison diagram 4(r) was of opposite sign but small. The same feature holds here as far as the $1s$-$2p$ correlation is considered. However, for the $2s$-$2p$ correlation, the contributions of diagrams 4(q) and 4(r) are of comparable order and opposite sign. The consequence of this is that the net $2s$-$2p$ correlation effect is opposite in sign to $1s$-$2p$, and there is substantial cancellation between the two. This makes the net (0, 2) dipolar contribution for beryllium relatively weak compared to lithium. A similar situation also holds for the magnetic-orbital interaction where there is again substantial cancellation between the $2s$-$2p$ and $1s$-$2p$ correlation contributions.

From the considerations of the contributions to the different types of hyperfine terms, it is clear that $2s$-$2p$ correlation effects play a decisive role in determining the relative sizes of the various orders. For the sake of comparison, when configuration-interaction calculations are available, we have listed in Table X the relative contributions from one-particle and two-particle excitations[17] through combinations of the contributions from the pertinent diagrams.

The only earlier theoretical calculations that have been performed on the hyperfine constant in Be ($^3P$) state are one electron in nature. One of these is an unrestricted Hartree–Fock procedure[18] (UHF) which was designed to include core-polarization contributions only for the contact interaction, since no angular excitations involving admixture of different $l$ states were incorporated. Since the UHF procedure involves self-consistency, to obtain a comparable result from our diagrams, one has to collect all diagrams that are one electron in nature. This number, namely, −113.390 MHz, listed in Table XI in the second column under the category "one-electron diagrams," was obtained by adding the (0, 0) and the higher-order one-electron contract contributions in Table X. The small difference between our diagrammatic one-electron result and the UHF result probably originates out of partial correlation effects included in the UHF procedure.

The other earlier result listed in Table XI involved the incorporation of core-polarization effects through the moment-perturbation (MP) procedure.[19] In this procedure, one perturbs the core $1s$ orbitals by the nuclear contact hyperfine interaction and then computes the exchange energy with the valence electrons using these perturbed orbitals. A comparable result can be obtained from our diagrammatic procedure by adding to the (0, 0) contribution, all (0, 1) diagram contributions including ladder corrections. The result one obtains

TABLE XI. Comparison of the present calculation with earlier theoretical results and experiment (in MHz).

| Method | $A_c$ | $A_d+A_o$ [a] | Total |
|---|---|---|---|
| UHF[b] | −113.5 | −8.8 | −122.3 |
| MP[c] | −111.9 | −8.8 | −120.7 |
| | Present calculation | | |
| One-electron diagrams | −113.390 | −8.634 | −122.024 |
| Core-polarization diagrams | −112.995 | ... | ... |
| Net including correlation | −115.224 | −8.982 | −123.206 ± 0.5 |
| | Experiment[d] | | |
| | −115.05 ± 0.4[e] | −8.49 ± 0.4 | |
| | −115.31 ± 0.4[f] | −9.23 ± 0.4 | −124.5368 ± 0.0017 |

[a]The results under UHF and MP for $A_d+A_o$ do not include core-polarization effects. But the diagrammatic calculations under core-polarization and one-electron diagrams do.

[b]See Ref. 18.

[c]See Ref. 19.

[d]See Ref. 8.

[e]Separation made using $A_d$ to $A_o$ ratio as −0.2.

[f]Separation made using $A_d$ to $A_o$ ratio as −0.213.

this way is seen to differ by only about 1 MHz from the MP result. This difference is most likely a consequence of a local approximation used in solving the first-order perturbation equations in the MP procedure.

In Table XI we have also listed the contributions to $A_d + A_o$ from core-polarization effects alone, as well as from all one-electron effects. The former would be comparable to the results including MP-type contributions for the dipolar effect, when available, while the latter would be suitable for comparison to the results of UHF-type calculations.[20]

In making a comparison between our calculated hyperfine constant and experiment, one needs to make two considerations, namely, the range of error in our nonrelativistic calculations and the importance of relativistic effects. The error limit of $\pm 0.5$ MHz quoted in Table XI is composed of three items. The first item is the over-all numerical accuracy of our computations which we conservatively estimate to involve a range of error $\pm 0.2$ MHz. The second item is connected with the role of higher-$l$ multipole components of $1/r_{12}$ for electron-electron interaction vertices beyond $f$ components which we believe involves an error range of $\pm 0.1$ MHz. Finally, one should include $\pm 0.2$ MHz due to the effect of higher-order diagrams.

As far as relativistic corrections are concerned, one can make a rough estimate of the relativistic correction to the direct (0, 0) $2s$ contribution using results of relativistic calculation[8] for lithium.[21] Taking account of the ratio of the magnetic moments of $Be^9$ and $Li^7$ leads to an estimated relativistic contribution of about $-0.3$ MHz. While the relativistic corrections to the core-polarization contribution and to $A_d + A_o$ are somewhat more difficult to estimate, together they are not expected to be larger in magnitude than $-0.1$ MHz. With these estimates of the relativistic contribution, the theoretical result is $-124.6$ MHz, which is in good agreement with experiment within the range of our error limit in Table XI.

As far as the individual contributions $A_c$, $A_d$, and $A_o$ to $A$ are concerned, unfortunately, no strictly experimental values are available to compare with our calculated nonrelativistic results in the last row of Table IX. The reason for this is that, while the number of constants is three, only two sets of data are available, namely, those for the total values of $A$ for $J=1$ and 2 states. However, Blachman and Lurio have used the one-electron value of $-0.2$ for the ratio of $A_d$ and $A_o$ to effect the separation of $A_c$ and $A_d + A_o$ leading to the values indicated in the first row under experiment in Table XI. While the agreement between the experimental values of $A_c$ and $A_d + A_o$ obtained this way and our theory is quite good, the agreement is further improved if one uses the ratio of $-0.213$ for $A_d/A_o$ which we have obtained from calculations (including correlation effects), to devise the values of $A_c$ and $A_d + A_o$ from experiment. These are listed in the last row of Table XI. It would be useful to have level-crossing data of the type available for the $^2P$ state of lithium to combine with the hyperfine data for $J=1$ and 2 states in order to obtain experimental values of $A_c$, $A_d$, and $A_o$ to compare with theory.

## ACKNOWLEDGMENTS

The authors are grateful to Dr. J. E. Rodgers for helpful discussions and the staff of the State University of New York at Albany Computing Center, for their helpful assistance.

---

*Work supported by National Science Foundation.

[1]J. Goldstone, Proc. R. Soc. Lond. A239, 267 (1957); K. A. Brueckner, Phys. Rev. **97**, 1353 (1955); Phys. Rev. **100**, 36 (1955); *The Many-Body Problem* (Wiley, New York, 1959); P. Noziéres, *Theory of Interacting Fermi Systems* (Benjamin, New York, 1964), Chap. V.

[2]E. S. Chang, T. P. Das, and R. T. Pu, Bull. Am. Phys. Soc. **12**, 69 (1967); E. S. Chang, R. T. Pu, and T. P. Das, Phys. Rev. **174**, 1 (1968).

[3]H. P. Kelly, Phys. Rev. **173**, 142 (1968).

[4]N. C. Dutta, C. Matsubara, R.T. Pu, and T. P. Das, Phys. Rev. **177**, 33 (1969).

[5]N.C. Dutta, C. Matsubara, R. T. Pu, and T. P. Das, Phys. Rev. Lett. **21**, 1139 (1968).

[6]J. D. Lyons, R. T. Pu, and T. P. Das, Phys. Rev. **178**, 103 (1969).

[7]T. Lee, N. C. Dutta, and T. P. Das, Phys. Rev. A **1**, 995 (1970).

[8]Arthur G. Blachman and Allen Lurio, Phys. Rev. **153**, 164 (1967).

[9]See Silvan S. Schweber, *An Introduction to Quantum Field Theory* (Harper and Row, New York, 1962), Chaps. 6 and 11.

[10]H. P. Kelly, Phys. Rev. **136**, B896 (1964).

[11]H. P. Kelly, Phys. Rev. **131**, 684 (1963).

[12]E. Clementi, IBM J. Res. Dev. **9**, 2 (1965).

[13]C. Froese, Can. J. Phys. **41**, 1895 (1963).

[14]A. Burgess, Proc. Phys. Soc. Lond. **442**, 81 (1963).

[15]B. N. Taylor, W. H. Parker, D. N. Langenberg, Rev. Mod. Phys. **41**, 375 (1969); N.M.R. Table, 5th ed. (Varian, New York, 1965), INS 1522A.

[16]Of the diagrams 1(i) through 1(l), only the contribution of 1(j) is listed in Table III, in view of our convention to present only those diagrams which contribute more than 0.25 MHz.

[17]For two- and three-particle excitations, we refer to dynamic correlations involving simultaneous excitations of those particles.

[18]D. A. Goodings, Phys. Rev. **123**, 1706 (1961).

[19]Wei-Mei Shyu, G. D. Gaspari, and T. P. Das, Phys. Rev. **141**, 603 (1966).

[20]Henry F. Schaeffer,III and Frank E. Harris, Phys. Rev. **167**, 67 (1968).

[21]L. Tterlikkis, S. D. Mahanti, and T. P. Das, Phys. Rev. **176**, 10 (1968).